Journal of Engineering Physics and Thermophysics, Vol. 75, No. 4, 2002

HEAT AND MASS FLUX EFFECTS ON A MOVING VERTICAL CYLINDER WITH CHEMICALLY REACTIVE SPECIES DIFFUSION

P. Ganesan and P. Loganathan

UDC 536.25

This paper presents the development of the free convection boundary layer flow of a viscous and incompressible fluid past an impulsively started semi-infinite vertical cylinder with uniform heat and mass fluxes and chemically reactive species. The governing coupled nonlinear partial differential equations have been solved numerically using the finite-difference scheme of Crank–Nicolson type. Graphical results for the velocity, temperature, concentration, local and average skin friction, Nusselt number and Sherwood number profiles are illustrated and discussed for various physical parametric values. It is noted that due to the presence of first-order chemical reaction the velocity decreases with increasing values of the chemical reaction parameter.

1. Introduction. Many transport processes exist in nature and in industrial applications in which simultaneous heat and mass transfer occurs as a result of combined buoyancy effects of thermal diffusion and diffusion of chemical species. The effects of mass transfer on flow past an impulsively started infinite vertical plate under constant heat flux condition along with chemical reactions were studied by Das et al. [1]. Exact solutions were derived by the Laplace transform technique. The authors observed that the skin friction is positive at large values of the chemical reaction parameter. It is applicable in chemical processing industries such as food processing and polymer production.

Several investigators studied the flow past a semi-infinite vertical cylinder. Yang [2] made a study of unsteady laminar free convection on vertical plates and cylinders to establish necessary and sufficient conditions under which similarity solutions are possible. On the basis of these conditions, all possible cases are derived, including those for unsteady conditions. Bottemanne [3] had studied such a problem for steady heat and mass flux conditions, both experimentally and theoretically. Chen and Yuh [4] dealt with steady combined heat and mass transfer effects for both conditions of uniform wall temperature/concentration and uniform heat/mass flux. Recently Heckel et al. [5] studied the steady free convection along slender vertical cylinders for variable surface heat flux conditions. Chen [6] investigated the steady free convection from a vertical needle with variable wall heat flux and found that there was a significant influence of its shape, size, and wall temperature variation upon the flow and heat transfer. Pop et al. [7] have studied the problem of a steady forced convection boundary layer of non-Newtonian fluids on a continuously moving cylinder.

In many industrial and environmental situations, transients do not start from quiescence, but from a previous heating and resulting flow condition. A solar collector panel is an example, when solar insulation suddenly changes, possibly due to changing cloud cover. An initial steady flow becomes a transient, which ultimately may result in another steady flow condition, as in the models of Ingham [8], Joshi and Gebhart [9], and Harris et al. [10, 11]. Several authors have analyzed laminar boundary-layer natural convection with uniform wall heat flux. Nagendra et al. [12] carried out a numerical study of steady boundary-layer equations for cylinders subjected to uniform heat flux and compared their predictions with the experimental results of their earlier study in water. Chambre and Young [13] had analyzed the problem of first-order chemical reactions in the neighborhood of a flat plate for destructive and generative reactions. In nature, pure air and water are not possible, since some foreign masses may be mixed with air and water. Takhar et al. [14] studied the combined heat and mass transfer along a moving cylinder with free stream using an implicit finite-difference scheme of Crank–Nicolson type. Ganesan and Loganathan [15] presented the unsteady flow past a moving semi-infinite vertical cylinder with heat and mass transfer.

School of Mathematics, Anna University, Chennai 600025, India; email: ganesan@annauniv.edu, ploknath@hotmail.com. Published in Inzhenerno-Fizicheskii Zhurnal, Vol. 75, No. 4, pp. 105–114, July–August, 2002. Original article submitted October 24, 2001.

1062-0125/02/7504-0899$27.00 ©2002 Plenum Publishing Corporation

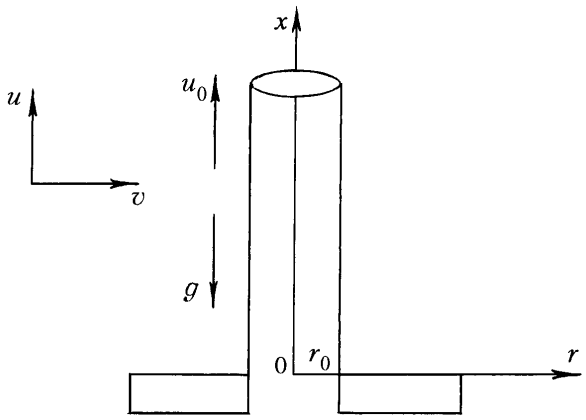

Fig. 1. The physical model and coordinate system.

In the present study, we consider the free convection flow over a vertical cylinder. Here we assume that a chemically reactive species is emitted from the surface of the cylinder and diffuses into the fluid. The reaction is assumed to take place entirely in the stream. In the present study, the concentration distribution of this particular component in the flow field is calculated. No analysis seems to have been presented for transient natural convection along vertical cylinders under uniform temperature/concentration along with chemical reaction. The main reason for the lack of study of this problem is due to difficult mathematical and numerical procedures in dealing with the non-similar boundary layers. The conservation equations of an unsteady laminar boundary layer are first transformed into a dimensionless form and their solutions are then obtained by an efficient implicit finite-difference scheme of Crank–Nicolson type.

2. Mathematical Analysis. Consider unsteady, laminar and incompressible viscous flow past a moving semi-infinite vertical cylinder of radius r_0 with uniform heat and mass fluxes. The physical model of the problem is shown in Fig. 1. Here the x-axis is taken along the axis of the cylinder in the vertically upward direction and the radial coordinate r is taken normal to it. The effect of viscous dissipation is assumed to be negligible. Initially, it is assumed that the cylinder and the fluid are at the same temperature T'_∞ and also at the same concentration C'_∞. At $t' \geq 0$, the cylinder starts to move in the vertical direction with constant velocity u_0.

A constant heat/mass flux ratio q_w/q_w^* is maintained at the surface of the cylinder. It is also assumed that there exists a homogeneous first-order chemical reaction between the fluid and species concentration. All physical properties are assumed to be constant except for the density in the buoyancy term, which is given by the usual Boussinesq approximation. The governing boundary-layer equations that are based on the balance laws of mass, linear momentum, and energy for this investigation can be written as

$$\frac{\partial (ru)}{\partial x} + \frac{\partial (rv)}{\partial r} = 0 , \tag{1}$$

$$\frac{\partial u}{\partial t'} + u\frac{\partial u}{\partial x} + v\frac{\partial u}{\partial r} = g\beta (T' - T'_\infty) + g\beta^* (C' - C'_\infty) + \frac{\upsilon}{r}\frac{\partial}{\partial r}\left(r\frac{\partial u}{\partial r}\right), \tag{2}$$

$$\frac{\partial T'}{\partial t'} + u\frac{\partial T'}{\partial x} + v\frac{\partial T'}{\partial r} = \frac{\alpha}{r}\frac{\partial}{\partial r}\left(r\frac{\partial T'}{\partial r}\right), \tag{3}$$

$$\frac{\partial C'}{\partial t'} + u\frac{\partial C'}{\partial x} + v\frac{\partial C'}{\partial r} = \frac{D}{r}\frac{\partial}{\partial r}\left(r\frac{\partial C'}{\partial r}\right) - K_l C' . \tag{4}$$

The appropriate boundary conditions for the velocity, temperature, and concentration are

$$t' \le 0: \quad u = 0, \quad v = 0, \quad T' = T'_\infty, \quad C' = C'_\infty \quad \text{for all} \quad x \ge 0 \quad \text{and} \quad r \ge r_0;$$

$$t' > 0: \quad u = u_0, \quad v = 0, \quad \frac{\partial T'}{\partial r} = -\frac{q_w}{k}, \quad \frac{\partial C'}{\partial r} = -\frac{q_w^*}{k} \quad \text{at} \quad r = r_0;$$

$$u = 0, \quad T' = T'_\infty, \quad C' = C'_\infty \quad \text{at} \quad x = 0 \quad \text{and} \quad r \ge r_0;$$

$$u \to 0, \quad T' \to T'_\infty, \quad C' \to C'_\infty \quad \text{as} \quad r \to \infty. \tag{5}$$

Introducing the dimensionless quantities

$$X = \frac{x\upsilon}{u_0 r_0^2}, \quad R = \frac{r}{r_0}, \quad U = \frac{u}{u_0}, \quad V = \frac{v r_0}{\upsilon}, \quad t = \frac{t'\upsilon}{r_0^2}, \quad C = \frac{C' - C'_w}{\frac{q_w^* r_0}{k}}, \quad T = \frac{T' - T'_w}{\frac{q_w r_0}{k}},$$

$$G_C = \frac{g\beta^* q_w^* r_0^3}{k\upsilon u_0}, \quad G_T = \frac{g\beta q_w r_0^3}{k\upsilon u_0}, \quad \mathrm{Sc} = \frac{\upsilon}{D}, \quad \mathrm{Pr} = \frac{\upsilon}{\alpha}, \quad K = \frac{uK_l}{r_0^2}, \tag{6}$$

we reduce Eqs. (1)–(4) to the following dimensionless form:

$$\frac{\partial (RU)}{\partial X} + \frac{\partial (RV)}{\partial R} = 0, \tag{7}$$

$$\frac{\partial U}{\partial t} + U\frac{\partial U}{\partial X} + V\frac{\partial U}{\partial R} = G_T + G_C + \frac{1}{R}\frac{\partial}{\partial R}\left(R\frac{\partial U}{\partial R}\right), \tag{8}$$

$$\frac{\partial T}{\partial t} + U\frac{\partial T}{\partial X} + V\frac{\partial T}{\partial R} = \frac{1}{\mathrm{Pr}\, R}\frac{\partial}{\partial R}\left(R\frac{\partial T}{\partial R}\right), \tag{9}$$

$$\frac{\partial C}{\partial t} + U\frac{\partial C}{\partial X} + V\frac{\partial C}{\partial R} = \frac{1}{\mathrm{Sc}\, R}\frac{\partial}{\partial R}\left(R\frac{\partial C}{\partial R}\right) - KC. \tag{10}$$

The corresponding initial and boundary conditions for dimensionless quantities are given by

$$t \le 0: \quad U = 0, \quad V = 0, \quad T = 0, \quad C = 0 \quad \text{for all} \quad X \ge 0 \quad \text{and} \quad R \ge 1;$$

$$t > 0: \quad U = 1, \quad V = 0, \quad \frac{\partial T}{\partial R} = -1, \quad \frac{\partial C}{\partial R} = -1 \quad \text{at} \quad R = 1;$$

$$U = 0, \quad T = 0, \quad C = 0 \quad \text{at} \quad X = 0;$$

$$U \to 0, \quad T \to 0, \quad C \to 0 \quad \text{at} \quad R \to \infty. \tag{11}$$

3. Numerical Procedure. In order to solve the unsteady, nonlinear coupled equations (7)–(10) under the boundary conditions (11), an implicit finite-difference scheme of Crank–Nicolson type has been employed. The region

*) The parameters G_T and G_C are related to thermal and mass Grashof numbers as follows: G_T = Gr/Re, G_C = Gr_C/Re, where Re = $u_0 r_0/\mathrm{n}\upsilon$.

of integration is considered as a rectangle with sides $X_{\max} = 1.0$ and $R_{\max} = 14.0$, where $R_{\max}$ corresponds to $R = \infty$, which lies very well outside the momentum, thermal, and concentration boundary layers. Appropriate mesh sizes $\Delta X = 0.02$, $\Delta R = 0.25$, and time step $\Delta t = 0.01$ are considered for the calculations. The finite-difference equations corresponding to Eqs. (7)–(10) are as follows:

$$\frac{U_{i,j-1}^{k+1} - U_{i-1,j-1}^{k+1} + U_{i,j}^{k+1} - U_{i-1,j}^{k+1} + U_{i,j-1}^{k} - U_{i-1,j-1}^{k} + U_{i,j}^{k} - U_{i-1,j}^{k}}{4\Delta X}$$

$$+ \frac{V_{i,j}^{k+1} - V_{i,j-1}^{k+1} + V_{i,j}^{k} - V_{i,j-1}^{k}}{2\Delta R} + \frac{V_{i,j}^{k+1}}{1 + (j-1)\,\Delta R} = 0\,, \tag{12}$$

$$\frac{U_{i,j}^{k+1} - U_{i,j}^{k}}{\Delta t} + \frac{U_{i,j}^{k}}{2\Delta X}\left(U_{i,j}^{k+1} - U_{i-1,j}^{k+1} + U_{i,j}^{k} - U_{i-1,j}^{k}\right) + \frac{V_{i,j}^{k}}{4\Delta R}\left(U_{i,j+1}^{k+1} - U_{i,j-1}^{k+1} + U_{i,j+1}^{k} - U_{i,j-1}^{k}\right)$$

$$= G_T \frac{T_{i,j}^{k+1} + T_{i,j}^{k}}{2} + G_C \frac{C_{i,j}^{k+1} + C_{i,j}^{k}}{2} + \frac{\left(U_{i,j-1}^{k+1} - 2U_{i,j}^{k+1} + U_{i,j+1}^{k+1} + U_{i,j-1}^{k} - 2U_{i,j}^{k} + U_{i,j+1}^{k}\right)}{2\,(\Delta R)^2}$$

$$+ \frac{\left(U_{i,j+1}^{k+1} - U_{i,j-1}^{k+1} + U_{i,j+1}^{k} - U_{i,j-1}^{k}\right)}{4\,[1 + (j-1)\,\Delta R]\,\Delta R}\,, \tag{13}$$

$$\frac{T_{i,j}^{k+1} - T_{i,j}^{k}}{\Delta t} + \frac{T_{i,j}^{k}}{2\Delta X}\left(T_{i,j}^{k+1} - T_{i-1,j}^{k+1} + T_{i,j}^{k} - T_{i-1,j}^{k}\right) + \frac{V_{i,j}^{k}}{4\Delta R}\left(T_{i,j+1}^{k+1} - T_{i,j-1}^{k+1} + T_{i,j+1}^{k} - T_{i,j-1}^{k}\right)$$

$$= \frac{\left(T_{i,j-1}^{k+1} - 2T_{i,j}^{k+1} + T_{i,j+1}^{k+1} + T_{i,j-1}^{k} - 2T_{i,j}^{k} + T_{i,j+1}^{k}\right)}{2\,(\Delta R)^2} + \frac{\left(T_{i,j+1}^{k+1} - T_{i,j-1}^{k+1} + T_{i,j+1}^{k} - T_{i,j-1}^{k}\right)}{4\,[1 + (j-1)\,\Delta R]\,\Delta R}\,, \tag{14}$$

$$\frac{C_{i,j}^{k+1} - C_{i,j}^{k}}{\Delta t} + \frac{C_{i,j}^{k}}{2\Delta X}\left(C_{i,j}^{k+1} - C_{i-1,j}^{k+1} + C_{i,j}^{k} - C_{i-1,j}^{k}\right) + \frac{V_{i,j}^{k}}{4\Delta R}\left(C_{i,j+1}^{k+1} - C_{i,j-1}^{k+1} + C_{i,j+1}^{k} - C_{i,j-1}^{k}\right)$$

$$= \frac{\left(C_{i,j-1}^{k+1} - 2C_{i,j}^{k+1} + C_{i,j+1}^{k+1} + C_{i,j-1}^{k} - 2C_{i,j}^{k} + C_{i,j+1}^{k}\right)}{2\,(\Delta R)^2}$$

$$+ \frac{\left(C_{i,j+1}^{k+1} - C_{i,j-1}^{k+1} + C_{i,j+1}^{k} - C_{i,j-1}^{k}\right)}{4\,[1 + (j-1)\,\Delta R]\,\Delta R} - \frac{K}{2}\left(C_{i,j}^{k+1} + C_{i,j}^{k}\right). \tag{15}$$

The thermal boundary condition

$$\frac{\partial T}{\partial R} = -1 \quad \text{at} \quad R = 1$$

in the finite-difference form is

$$\frac{1}{2\Delta R}\left(T_{i,2}^{k+1}+T_{i,2}^{k}-T_{i,0}^{k+1}-T_{i,0}^{k}\right)=-1\,,$$

i.e.,

$$T_{i,2}^{k+1}+T_{i,2}^{k}+2\Delta R=T_{i,0}^{k+1}+T_{i,0}^{k}\,. \tag{16}$$

At $R=1$ (i.e., $j=1$), Eq. (14) becomes

$$\frac{T_{i,1}^{k+1}-T_{i,1}^{k}}{\Delta t}+\frac{U_{i,1}^{k}}{2\Delta X}\left(T_{i,1}^{k+1}-T_{i-1,1}^{k+1}+T_{i,1}^{k}-T_{i-1,1}^{k}\right)+\frac{V_{i,1}^{k}}{4\Delta R}\left(T_{i,2}^{k+1}-T_{i,0}^{k+1}+T_{i,2}^{k}-T_{i,0}^{k}\right)$$

$$=\frac{T_{i,0}^{k+1}-2T_{i-1,1}^{k+1}+T_{i,2}^{k+1}+T_{i,0}^{k}-2T_{i-1,1}^{k}+T_{i,2}^{k}}{2\,\mathrm{Pr}\,(\Delta R)^{2}}+\frac{T_{i,2}^{k+1}-T_{i,0}^{k+1}+T_{i,2}^{k}-T_{i,0}^{k}}{4\,\mathrm{Pr}\,\Delta R}\,. \tag{17}$$

After eliminating $T_{i,0}^{k+1}+T_{i,0}^{k}$ and using Eq. (16), we reduce Eq. (17) to the form

$$\frac{T_{i,1}^{k+1}-T_{i,1}^{k}}{\Delta t}+\frac{U_{i,1}^{k}}{2\Delta X}\left(T_{i,1}^{k+1}-T_{i-1,1}^{k+1}+T_{i,1}^{k}-T_{i-1,1}^{k}\right)-\frac{V_{i,1}^{k}}{2\Delta R}$$

$$=\frac{1}{\mathrm{Pr}\,(\Delta R)^{2}}\left(T_{i,2}^{k+1}+T_{i,2}^{k}-T_{i,2}^{k+1}-T_{i,1}^{k}+\Delta R\right)-\frac{1}{2\,\mathrm{Pr}}\,. \tag{18}$$

Similarly,

$$C_{i,2}^{k+1}+C_{i,2}^{k}+2\Delta R=C_{i,0}^{k+1}+C_{i,0}^{k}\,. \tag{19}$$

At $R=1$ (i.e., $j=1$), Eq. (18) becomes

$$\frac{C_{i,1}^{k+1}-C_{i,1}^{k}}{\Delta t}+\frac{U_{i,1}^{k}}{2\Delta X}\left(C_{i,1}^{k+1}-C_{i-1,1}^{k+1}+C_{i,1}^{k}-C_{i-1,1}^{k}\right)+\frac{V_{i,1}^{k}}{4\Delta R}\left(C_{i,2}^{k+1}-C_{i,0}^{k+1}+C_{i,2}^{k}-C_{i,0}^{k}\right)$$

$$=\frac{C_{i,0}^{k+1}-2C_{i-1,1}^{k+1}+C_{i,2}^{k+1}+C_{i,0}^{k}-2C_{i-1,1}^{k}+C_{i,2}^{k}}{2\,\mathrm{Pr}\,(\Delta R)^{2}}+\frac{C_{i,2}^{k+1}-C_{i,0}^{k+1}+C_{i,2}^{k}-C_{i,0}^{k}}{4\,\mathrm{Pr}\,\Delta R}-\frac{K}{2}\left(C_{i,1}^{k+1}+C_{i,1}^{k}\right). \tag{20}$$

After eliminating $C_{i,0}^{k+1}+C_{i,0}^{k}$ and using Eq. (19), we reduce Eq. (20) to the form

$$\frac{C_{i,1}^{k+1}-C_{i,1}^{k}}{\Delta t}+\frac{U_{i,1}^{k}}{2\Delta X}\left(C_{i,1}^{k+1}-C_{i-1,1}^{k+1}+C_{i,1}^{k}-C_{i-1,1}^{k}\right)-\frac{V_{i,1}^{k}}{2\Delta R}=$$

$$=\frac{1}{\mathrm{Pr}\,(\Delta R)^{2}}\left(C_{i,2}^{k+1}+C_{i,2}^{k}-C_{i,2}^{k+1}-C_{i,1}^{k}+\Delta R\right)-\frac{1}{2\,\mathrm{Pr}}-\frac{K}{2}\left(C_{i,1}^{k+1}+C_{i,1}^{k}\right). \tag{21}$$

Here i and j designate the grid points along the X- and R-directions respectively and the superscript k designates a value of time $k\Delta t$. During any one-time step, the coefficients $U_{i,j}^{k}$ and $V_{i,j}^{k}$ appearing in Eqs. (12), (13), (18), and (21) are treated as constants. The values of U, V, T, and C are known at time $t=0$ from the initial conditions. The values of U, V, T, and C at the next time step $t=\Delta t$ are calculated as follows.

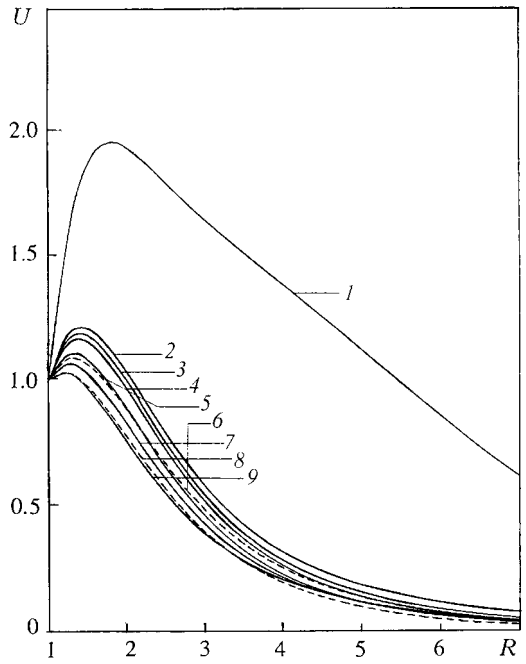

Fig. 2. Steady state velocity profiles at $X = 1.0$ for $\mathrm{Pr} = 0.71$ (solid curves) and 7 (dashed curves): 1) $K = -2$, $\mathrm{Sc} = 0.6$, and $t = 13.35$; 2) –0.2, 0.6, and 13.66; 3) 0, 0.6, and 9.99; 4) 0.2, 0.6, and 8.73; 5) 1, 0.6, and 9.43; 6) 0.2, 0.6, and 8.71; 7) 2, 0.6, and 10.41; 8) 1, 0.6, and 7.67; 9) 0.2, 2, and 11.25.

Equation (21) at every internal nodal point on a particular *i*th level constitutes a tridiagonal system of equations, which is solved by the Thomas algorithm described by Carnahan et al. [16]. Thus the values of C are known at every nodal point on a particular *i*th level at $t = \Delta t$. Similarly the values of T are calculated from Eq. (18). Using the values of C and T in Eq. (13), values of U are calculated. Then the values of V are calculated explicitly by using Eq. (12) at every nodal point on a particular *i*th level at the $(n+1)$th time level. Computations are repeated until the steady state is reached. This process is repeated for various *i*th levels. Thus, the values of C, T, U, and V are known at all grid points in the rectangular region at the $(n+1)$th time level. The steady-state solution is assumed to have been reached when the absolute differences between values of velocity U and temperature T as well as concentration C at two consecutive time steps are less than 10^{-5} at all grid points.

After experimenting with a number of mesh sizes, the mesh sizes have been fixed as $\Delta X = 0.02$ and $\Delta R = 0.2$ with time step $\Delta t = 0.01$. In this case, spatial mesh sizes are reduced by 50% in one direction and later in both directions, and results are compared. It is observed that, when the mesh size is reduced by 50% in the R-direction, the results differ in the fifth place after the decimal point, while for the mesh sizes reduced by 50% in the X-direction or in both directions the results are correct to fourth decimal places. Hence, the above mesh sizes have been considered as appropriate.

4. Results and Discussion. In order to get a clear insight of the physical problem, numerical results are displayed with the help of graphical illustrations. We consider a homogeneous first-order chemical reaction. The diffusing species either can be destroyed or generated in the homogeneous reaction. The chemical reaction parameter can be adjusted to meet these circumstances if one takes (i) $K > 0$ for a destructive reaction, (ii) $K < 0$ for a generative reaction, and (iii) $K = 0$ for no reaction. Solutions are obtained for various physical parameters such as thermal Grashof number, mass Grashof number, Prandtl number, chemical reaction parameter, and Schmidt number.

The steady-state velocity profiles at $X = 1.0$ for different values of chemical reaction parameter K, Prandtl number Pr, and Schmidt number Sc are shown in Fig. 2. It is noted that the velocity increases with decreasing values of Schmidt number, Prandtl number, and chemical reaction parameter. The time required to reach the steady state increases with increasing Schmidt number and chemical reaction parameter. This shows that the contribution of mass diffusion to the buoyancy force increases the maximum velocity significantly.

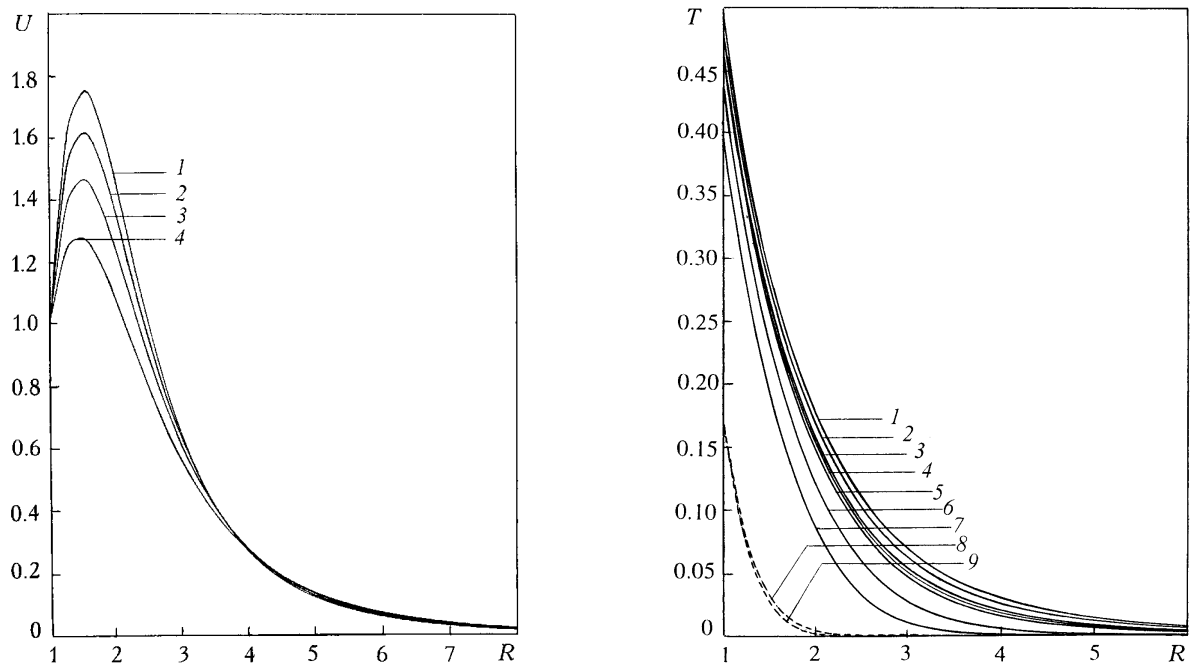

Fig. 3. Steady state velocity profiles at $X = 1$ for $\mathrm{Pr} = 0.71$, $\mathrm{Sc} = 0.6$, and $K = 0.2$: 1) $G_T = 15$, $G_C = 10$, and $t = 7.63$; 2) 10, 10, and 7.78; 3) 5, 10, and 7.92; 4) 5, 5, and 8,6.

Fig. 4. Transient and steady state temperature profiles at $X = 1$ for $G_T = 2$, $G_C = 5$, $\mathrm{Sc} = 0.6$, $\mathrm{Pr} = 0.71$ (solid curves) and 7 (dashed curves): 1) $K = 2$ and $t = 10.41$; 2) 1 and 9.43; 3) 0.2 and 8.73; 4) 0 and 9.99; 5) –0.2 and 13.66; 6) –1 and 18.73; 7) –2 and 13.35; 8) –0.2 and 1.2 (temporal maximum); 9) –0.2 and 8.71.

For the case of $K > 0$, i.e., for a destructive reaction, increasing values of K leads to a fall in velocity profiles. For a generative reaction, $K < 0$, a fall in velocity is also observed for increasing K. This is due to the fact that as $K < 0$, the last term in the concentration equation becomes positive and plays a crucial role. The steady-state velocity profiles for different G_T and G_C are shown in Fig. 3. It is observed that the velocity increases with G_T and G_C.

The transient and steady-state temperature profiles for different values of Prandtl number and chemical reaction parameter are shown in Fig. 4. The effect of Prandtl number is very important in the temperature field. The thermal boundary-layer thickness decreases with increasing Prandtl number. It is observed that the temperature increases with increasing values of the chemical reaction parameter.

The steady-state concentration profiles for different chemical reaction parameter and Schmidt number are shown in Fig. 5. The effects of the chemical reaction parameter and Schmidt number are very important in the concentration profiles. It is observed that there is a fall in concentration due to increasing values of the chemical reaction parameter or Schmidt number. This is due to the fact that a larger Sc corresponds to a thinner concentration boundary layer relative to the momentum boundary layer. This results in a larger concentration gradient on the cylinder.

The local as well as average skin friction, Nusselt number, and Sherwood number in terms of dimensionless quantities are given by

$$\tau_x = -\left.\frac{\partial U}{\partial R}\right|_{R=1}, \tag{22}$$

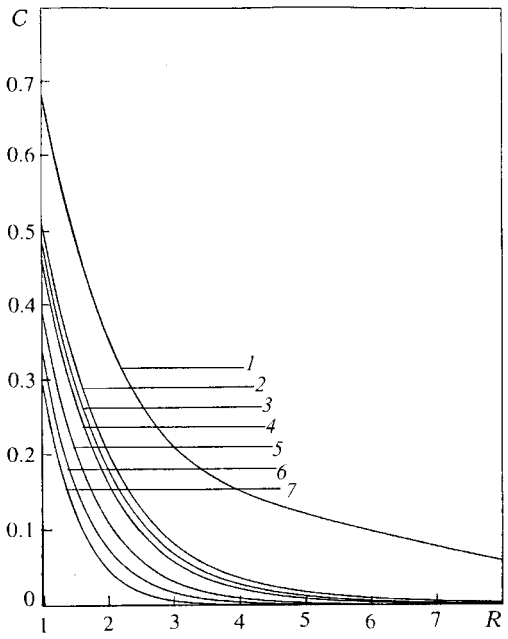

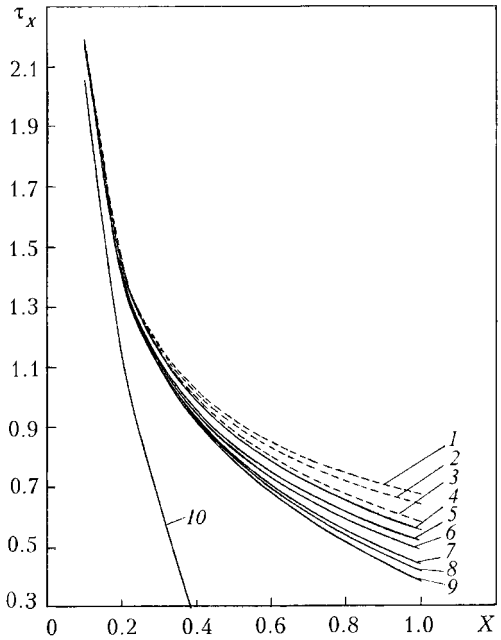

Fig. 5. Steady state concentration profiles at $X = 1$ for $G_T = 2$, $G_C = 5$, and $\mathrm{Pr} = 0.71$: 1) $K = -1$, $\mathrm{Sc} = 0.6$, and $t = 18.73$; 2) –0.2, 0.6, and 13.66; 3) 0, 0.6, and 9.99; 4) 0.2, 0.6, and 8.73; 5) 1, 0.6, and 9.43; 6) 2, 0.6, and 10.41; 7) 0.2, 2, and 11.25.

Fig. 6. Local skin friction for $G_T = G_C = 0.5$, $\mathrm{Pr} = 0.71$ (solid curves) and 7 (dashed curves): 1) $K = 2$ and $\mathrm{Sc} = 0.6$; 2) 1 and 0.6; 3) 0.2 and 0.6; 4) 1 and 2; 5) 2 and 0.6; 6) 1 and 0.6; 7) 0.2 and 0.6; 8) 0 and 0.6; 9) –0.2 and 0.6; 10) –2 and 0.6.

$$\bar{\tau} = -\int_0^1 \left.\frac{\partial U}{\partial R}\right|_{R=1} dX \,, \tag{23}$$

$$\mathrm{Nu}_x = -X \left.\frac{\partial T}{\partial R}\right|_{R=1} \,, \tag{24}$$

$$\overline{\mathrm{Nu}} = -\int_0^1 \left.\frac{\partial T}{\partial R}\right|_{R=1} dX \,, \tag{25}$$

$$\mathrm{Sh}_x = -\frac{X \left.\dfrac{\partial C}{\partial R}\right|_{R=1}}{C\big|_{R=1}} \,, \tag{26}$$

$$\mathrm{Sh} = -\int_0^1 \frac{\left.\dfrac{\partial C}{\partial R}\right|_{R=1}}{C\big|_{R=1}} dX \,. \tag{27}$$

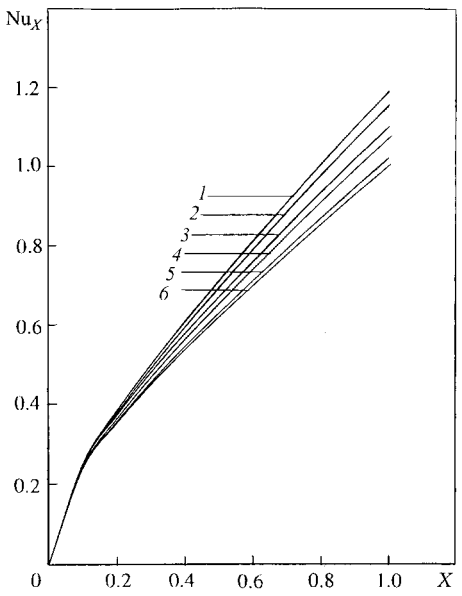

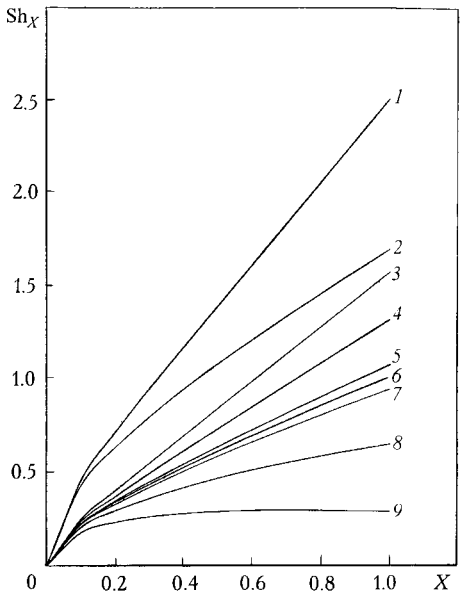

Fig. 7. Local Nusselt number for $\mathrm{Pr} = 0.71$ and $K = 0.2$: 1) $G_T = 10$, $G_C = 10$, and $\mathrm{Sc} = 0.6$; 2) 5, 10, and 0.6; 3) 2, 2, and 0.16; 4) 2, 5, and 0.6; 5) 2, 2, and 0.6; 6) 2, 5, and 2.

Fig. 8. Local Sherwood number for $\mathrm{Pr} = 0.71$, $G_T = 2$, and $G_C = 5$: 1) $K = 2$ and $\mathrm{Sc} = 2$; 2) 2 and 0.2; 3) 2 and 0.6; 4) 1 and 0.6; 5) 0.2 and 0.6; 6) 0 and 0.6; 7) –0.2 and 0.6; 8) –1 and 0.6; 9) –2 and 0.6.

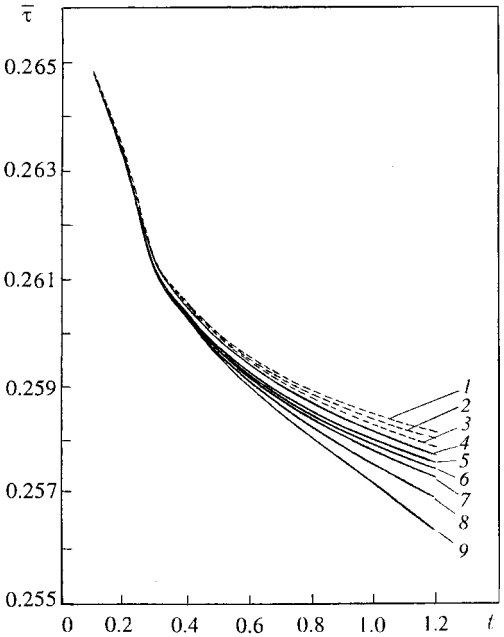

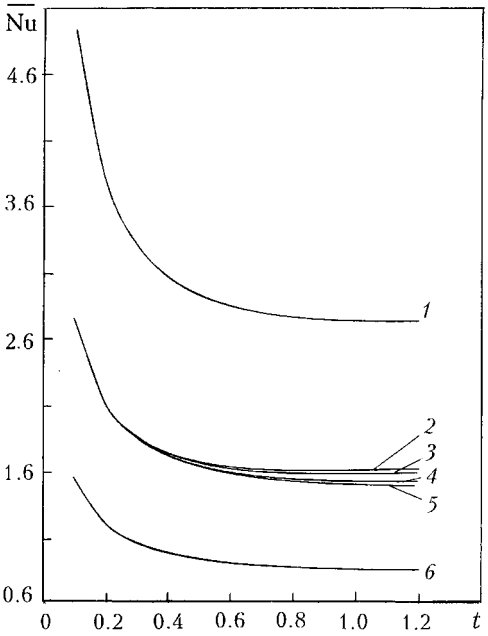

Fig. 9. Average skin friction for $G_T = G_C = 0.5$, $\mathrm{Pr} = 0.71$ (solid curves) and 7 (dashed curves): 1) $K = 2$ and $\mathrm{Sc} = 0.6$; 2) 1 and 0.6; 3) 0.2 and 0.6; 4) 0.2 and 2; 5) 2 and 0.6; 6) 1 and 0.6; 7) 0.2 and 0.6; 8) –1 and 0.6; 9) –2 and 0.6.

Fig. 10. Average Nusselt number for $\mathrm{Pr} = 0.71$, $K = 2$: 1) $G_T = 2$, $G_C = 5$, and $\mathrm{Sc} = 2$; 2) 10, 10, and 0.6; 3) 5, 10, and 0,6; 4) 2, 5, and 0.6; 5) 2, 2, and 0.6; 6) 2, 2, and 0.16.

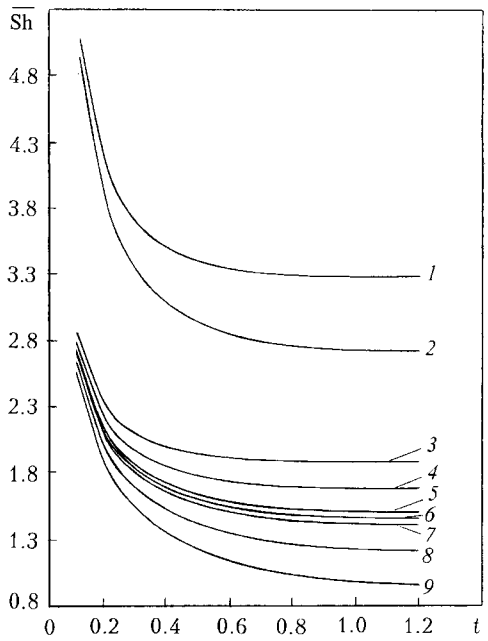

Fig. 11. Average Sherwood number for $\mathrm{Pr} = 0.71$, $G_T = 2$, and $G_C = 5$: 1) $K = 2$ and $\mathrm{Sc} = 2$; 2) 0.2 and 2; 3) 2 and 0.6; 4) 1 and 0.6; 5) 0.2 and 0.6; 6) 0 and 0.6; 7) −0.2 and 0.6; 8) −1 and 0.6; 9) −2 and 0.6.

The derivatives involved in Eqs. (22)–(27) are evaluated by a five-point approximation formula and integrals are evaluated through the use of the Newton–Cotes formula.

The local skin-friction profiles for different chemical reaction parameters and Schmidt numbers are plotted in Fig. 6 as functions of axial coordinate X. The local skin friction decreases as X increases. It is noted that the local shear stress increases with increasing values of the chemical reaction parameter and Schmidt number. The local Nusselt number for different G_T, G_C, and Sc are presented in Fig. 7. It is observed that the rate of heat transfer increases with increasing values of G_T or G_C. The local Sherwood numbers for different values of Sc and K are shown in Fig. 8 at steady state. They increase as the axial coordinate and Schmidt number increase. This is due to the fact that for a generative reaction the rate of mass transfer increases as Sc and the reaction parameter increase but the opposite effect has been observed for a destructive reaction.

The average skin friction, Nusselt number, and Sherwood number are shown in Figs. 9–11 respectively as functions of time at $X = 1.0$ for various parameters. Figure 9 shows that the shear stress increases with increasing values of K and Sc. Initially, higher values of the average Nusselt and Sherwood numbers are observed and then they decrease with time. From Fig. 10 it is observed that the average heat-transfer rate increases for increasing G_T, G_C, and Sc. In the initial time steps, the rate of heat transfer is the same for fixed values of Sc. In Fig. 11, the average Sherwood number is also the same initially for fixed values of Sc. This shows that there is only mass diffusion in the initial time level. Larger values of K or Sc correspond to higher values of Sherwood numbers.

5. Conclusions. A numerical study has been carried out for the flow past an impulsively started semi-infinite isothermal vertical cylinder with constant heat and mass fluxes and diffusion of chemical reactive species. A system of governing partial differential equations is solved by an implicit finite-difference scheme of Crank–Nicolson type. The fluids considered in this paper are both air and water. The results are obtained for different values of thermal Grashof number, mass Grashof number, Schmidt number, and chemical reaction parameter. Conclusions of this study are as follows:

1. The time required to reach the steady state increases with increasing Schmidt number Sc. For both generative and destructive reactions this time increases as the chemical reaction parameter K increases.

2. The momentum boundary layer increases with decreasing values of Sc and Pr. It is observed that there is a rise in the velocity due to the presence of mass diffusion.

3. The thermal boundary-layer thickness increases with decreasing value of K.

4. For both generative and destructive reactions, temperature increases, but the velocity and concentration decrease with increasing chemical reaction parameter.

The authors wish to acknowledge support for this research work from the CSIR (Council of Scientific and Industrial Research) through the award of Senior Research Fellowship to the second author.

NOTATION

C', species concentration; C, dimensionless species concentration; D, binary diffusion coefficient; Gr, thermal Grashof number; Gr_C, mass Grashof number; g, acceleration due to gravity; K, chemical reaction parameter; K_l, dimensional chemical reaction parameter; k, thermal conductivity; q_w, heat flux; q_w^*, mass flux of the diffusing species; $\overline{\mathrm{Nu}}$, average Nusselt number; Nu_x, local Nusselt number; Pr, Prandtl number; R, dimensionless radial coordinate; r, radial coordinate; r_0, radius of cylinder; Sc, Schmidt number; $\overline{\mathrm{Sh}}$, average Sherwood number; Sh_x, local Sherwood number; T', temperature; T, dimensionless temperature; t', time; t, dimensionless time; U and V, dimensionless velocity components in X and R directions respectively; u and v, velocity components in x and r directions respectively; x, axial coordinate measured vertically; X, dimensionless axial coordinate; α, thermal diffusivity; β, volumetric coefficient of thermal expansion; β^*, volumetric coefficient of expansion with concentration; υ, kinematic viscosity; ρ, density; τ_x, local skin friction; $\bar{\tau}$, average skin friction. Subscripts: w, wall; ∞, the free stream condition. Superscripts: k, time step level.

REFERENCES

1. U. N. Das, R. Deka, and V. M. Soundalgekar, *Eng. Res.*, **60**, 284–290 (1994).
2. K.T. Yang, *J. Appl. Mech.*, **27**, 230–236 (1960).
3. G. A. Bottemanne, *Appl. Sci. Res*., **25**, 372–382 (1972).
4. T. S. Chen and C. F. Yuh, *Int. J. Heat Mass Transfer*, **23**, 451–461 (1980).
5. J. J. Heckel, T. S. Chen, and B. F. Armaly, *Trans. ASME, C*, **111**, 1108–1111 (1989).
6. J. L. S. Chen, *Trans. ASME, C*, **105**, 403–406 (1983).
7. I. Pop, M. Kumari, and G. Nath, *Int. J. Engng. Sci*., **28**, 303–312 (1990).
8. D. B. Ingham, *Int. J. Heat Mass Transfer*, **27**, 1837–1843 (1984).
9. Y. Joshi and B. Gebhart, *Int. J. Heat Mass Transfer*, **31**, 743–757 (1998).
10. S. D. Harris, D. B. Ingham, and I. Pop, *Trans. J. Porous Media*, **26**, 207–226 (1997).
11. S. D. Harris, D. B. Ingham, and I. Pop, *Fluid Dyn. Res*., **18**, 313–324 (1996).
12. H. R. Nagendra, M. A. Tirunarayanan, and A. Ramachandran, *Trans. ASME, C*, **92**, 191–194 (1970).
13. P. L. Chambre and J. D. Young, *Phys. Fluids*, **1**, 48–51 (1958).
14. H. S. Takher, A. J. Chamkha, and G. Nath, *Heat Mass Transfer*, **36**, 237–246 (2000).
15. P. Ganesan and P. Loganathan, *Heat Mass Transfer*, **37,** No. 1, 59–65 (2001).
16. B. Carnahan, H. A. Luther, and J. O. Wilkes, in: *Applied Numerical Methods*, John Wiley and Sons, New York (1969), p. 44.